PCCP

Structural and vibrational characterization of methyl glycolate in the low temperature crystalline and glassy states

Susana Jarmelo, Teresa M. R. Maria, Maria Luísa P. Leitão and Rui Fausto*

Departamento de Química, Universidade de Coimbra, P-3049 Coimbra, Portugal.
E-mail: RFausto@gemini.ci.uc.pt

Received 24th November 1999, Accepted 10th January 2000

The low temperature phases of methyl glycolate (**MGly**) were identified and characterized structurally by differential scanning calorimetry, infrared and Raman spectroscopies and molecular modeling. Within the temperature range 13–273 K, **MGly** may exist in three solid phases. A crystalline phase (**I**) can be formed from the liquid upon slow cooling [T_{onset} = 222–227 K] or from the low temperature glassy state resulting from fast deposition of the vapour onto a cold substrate at 13 K and subsequent warming. A mixture of the glassy state and crystalline phase (**I**) is obtained by cooling the liquid at higher cooling rates ($v_{cooling} \geqslant 10$ K min^{-1}). Upon heating this mixture, devitrification occurs at *ca.* 175 K, the cold liquid then formed giving rise to a second crystalline variety (**II**) at T_{onset} = 198–207 K. In the glassy state, individual **MGly** molecules may assume the two conformational states previously observed for this compound isolated in an argon matrix and in the liquid phase [S. Jarmelo and R. Fausto, *J. Mol. Struct.*, 1999, **509**, 183]. On the contrary, the crystalline phase **I** was found to exhibit conformational selectivity—in this phase, all individual molecules assume a conformation analogous to the most stable conformer found for the isolated molecule and in the liquid (the *syn-syn* s-*cis* conformer, where the H–O–C–C, O–C–C=O and O=C–O–C dihedrals are *ca.* 0°). In agreement with the spectroscopic results, a molecular modeling analysis reveals that, in this phase, two non-equivalent molecules exhibiting an *intra*molecular OH···O= hydrogen bond exist, which are connected by a relatively strong *inter*molecular OH···O′= hydrogen bond. Crystalline state **II** could not be characterized in detail structurally, but the thermodynamic studies seem to indicate that it corresponds to a metastable crystalline form having a more relaxed structure and a slightly higher energy than crystalline state **I**. The observed temperature of fusion for the two observed crystalline forms are: **I**, 264 K and **II**, 260 K.

1. Introduction

Methyl glycolate (**MGly**) is the simplest α-hydroxy carboxylic ester. In the last few years, this family of compounds, as other families of α-hydroxy substituted carboxylic compounds, has drawn the attention of many people, due to its important medical and pharmaceutical applications.[1–4] The use of α-hydroxy substituted carboxylic compounds in dermatology and the cosmetics industry is well known,[1,2] but these substances are also currently used as inhibitors of harmful oxidation biochemical processes,[3] and important research is presently going on in order to develop new materials based on biodegradable polymers derived from these compounds that can be used for reconstruction of biological tissues and in organ transplantation.[5] In addition, these molecules also play an important role as precursors of polymeric materials currently used for different applications.[6]

Contrarily to glycolic acid, which has been extensively studied, both experimentally and theoretically,[7–10] **MGly** has not been paid much attention. Previously, **MGly** was studied theoretically[11–13] and experimentally in the gaseous phase, in solution and isolated in solid argon,[13–17] but there is a lack of experimental information regarding its liquid and solid phases. Recently, using a multidisciplinary approach, where conventional infrared and Raman spectroscopies in the liquid phase at room temperature, matrix isolation infrared spectroscopy and quantum chemical calculations were used, we reported the structures, relative energies and vibrational spectra of the most stable conformers of monomeric **MGly**.[17] We have found that, both in the isolated molecule situation and in the liquid, this molecule exists in two experimentally detectable conformational states: the *syn-syn* s-*cis* conformer (**Ss**; see Fig. 1), which exhibits an intramolecular OH···O= hydrogen bond and is the most stable form, and the doubly degenerated by symmetry *gauche-skew* s-*cis* conformer (**Gsk**; dihedral angles H–O–C–C, O–C–C=O and O=C–O–C of 48.5°, 155.0° and 0.0°, respectively, see also Fig. 1) which has an energy 9.5 kJ mol^{-1} higher than the conformational ground state, in the gaseous phase.[17]

In the present study, structural, thermodynamics and vibrational data for the solid phases (glassy and crystalline) and phase transitions of **MGly** within the temperature range 13–273 K are reported. Differential scanning calorimetry was used to detect and characterize low temperature phase transitions and vibrational spectroscopy (both Raman and infrared) was used to shed light on the nature of the different

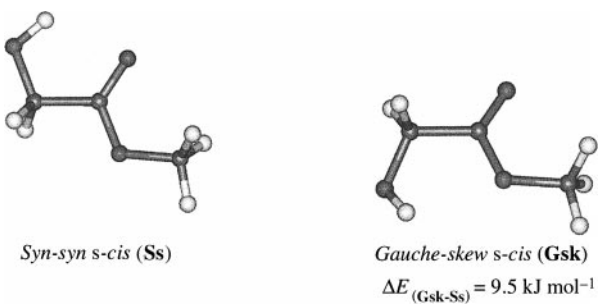

Fig. 1 Most stable conformers of methyl glycolate.

phases observed. Theoretical results obtained from quantum chemical calculations[17] or from molecular modeling were used to help interpretation of the vibrational data and to characterize the main intermolecular interactions present in the spectroscopically observed crystalline phase. Finally, a temperature variation study of the liquid phase spectra of **MGly**, within the temperature range 273–373 K, was also undertaken, in order to improve the available description of the conformational equilibrium in this phase. Note that the **Gsk**/**Ss** population ratio in the liquid phase at 298 K was previously estimated taking only into consideration the comparison between the calculated and observed relative intensities of the νC–C stretching Raman bands originated in each conformer at this temperature.[17] The estimated **Gsk**/**Ss** population ratio obtained by this way (0.457) indicates that conformer **Gsk** is stabilized in the liquid phase when compared with the isolated molecule situation. Such a result may be related with the ability of this conformer to establish stronger *inter*molecular hydrogen bonds than the **Ss** form, since it does not show the considerably strong *intra*molecular OH···O= hydrogen bond that is present in the latter conformer. An experimental value for the **Gsk**/**Ss** population ratio in the liquid phase, at 298 K, obtained from a Van't Hoff plot, is now reported.

2. Experimental

Methyl glycolate was obtained commercially (spectroscopic grade) and used without any additional purification.

Infrared spectra were obtained using a Mattson (Infinity Series) or a Bomem (MB104) Fourier transform spectrometer equipped with a deuterated triglycine sulfide (DTGS) detector and Ge/KBr or Zn/Se optics. Data collection was performed with 1 cm^{-1} spectral resolution. Band intensities were obtained from the area of the observed peaks, subjected to previous deconvolution by using the peak fitting module of ORIGIN 4.0.[18]

The solid state samples were prepared as a thin film by spraying the necessary amount of vapour of **MGly**, previously contained in an air-purged glass tube which was directly connected to the cryostat by a flux controlling valve, onto a KBr window, cooled using an APD cryogenics DMX closed cycle helium refrigeration system whose principal component is a DE-202 Displex expander. The refrigeration system is supported by an APD cryogenics Helium compressor (model HC-2D-1) and is connected to a high efficiency vacuum system whose main component is an Alcatel PTR5001 turbomolecular pump. The deposition temperature, measured at the window with a Pt100 sensor and a Scientific Instruments digital temperature controller (model 9650), was 13 K. For liquid phase studies, data collection was performed using a specially designed dismountable transmission variable temperature cell with KBr windows, linked to a T48 (Red Lion Controls) temperature controller. In all cases, the error in temperature measurements was less than 1 degree.

Raman spectra were obtained using a SPEX 1403 double monochromator spectrometer (focal distance 0.85 m, aperture *f*/7.8), equipped with holographic gratings with 1800 grooves mm^{-1} (ref. 1800-1SHD). The 514.5 nm argon laser (Spectra-Physics, model 164-05) line, adjusted to provide 220 mW power at the sample, was used as excitation radiation. Detection was effected using a thermoelectrically cooled Hamamatsu R928 photomultiplier. Spectra were recorded using increments of 1 cm^{-1} and integration times of 1 s. The sample was sealed into a glass capillary tube which is inserted within a Harney–Miller cell.[19] The cell was then cooled using a continuous flux liquid nitrogen refrigeration system equipped with an Alcon electrovalve (model 68252412) which enables precise control of the nitrogen flux reaching the cell. The temperature is controlled by a T48 (Red Lion Controls) temperature controller, the experimental error in the measured temperature being *ca.* 1–2 degrees within the range of temperatures covered.

Thermal studies were carried out with a Perkin-Elmer differential scanning calorimeter (Pyris-1), over the temperature range 113–283 K. Scanning rates ranging from 2 to 10 K min^{-1} were used. For cooling, the Perkin-Elmer liquid nitrogen cooling system CryoFill-1 was used. The samples (*ca.* 4 mg) were pressed in aluminium pans suitable for volatile substances. Temperature calibration was performed between 113 and 283 K with high grade cyclopentane and cyclohexane (Merck, reference substances for gas chromatography) and *n*-decane (Sigma, 99+%). For heat calibration, the enthalpy of the glass transition of cyclohexane occurring at 186.25 K[20] was used.

Molecular modeling studies were undertaken with the CFF95 force field[21] and the *Cerius*[2] (version 3.5) molecular modeling package[22] using the program standard convergence criteria and optimization algorithms.

3. Results and discussion

3.1. Differential scanning calorimetry (DSC) studies

Fig. 2 presents DSC heating curves corresponding to samples of **MGly** previously cooled using different cooling rates. The upper curve (a) was obtained by heating a sample previously submitted to slow cooling (−2 K min^{-1}), whilst the bottom curve (b) corresponds to a sample previously cooled using a faster cooling rate (−10 K min^{-1}). Both curves result from heating the sample at a constant rate of 2 K min^{-1}. Table 1 presents some relevant data extracted from these curves.

The single peak observed in the heating curve (a) (T_{onset} = 264 ± 1.8 K; T_{peak} = 270 ± 1.6 K) corresponds to the fusion of a crystalline phase ($\Delta_{fus}H$ = 11.4 ± 0.80 kJ mol^{-1}), hereafter named crystal **I**. This crystalline phase can be obtained by crystallization of the liquid, upon slow cooling, at a temperature of 224 ± 2.3 K. No significant changes of heat capacity could be observed in either the heating or the cooling curves of this sample, clearly indicating that, in this case, complete crystallization occurred. In addition, since the crystallization peak exhibits a complex structure and the fusion peak shows a clearly asymmetric profile, the results seem to

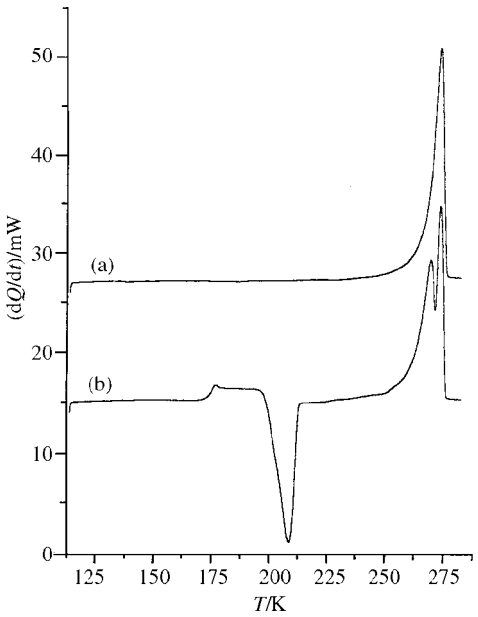

Fig. 2 DSC heating curves of a sample of methyl glycolate previously submitted to (a) slow cooling (−2 K min^{-1}) and (b) fast cooling (−10 K min^{-1}). Both curves were obtained at a constant heating rate of 2 K min^{-1}.

Table 1 Relevant thermodynamic data for methyl glycolate obtained from DSC measurements

Cooling rate:	-2 K min^{-1}	-10 K min^{-1}
Heating rate:	2 K min^{-1}	2 K min^{-1}
Glass transition		
T_g		174.6 ± 0.42 K
ΔC_p		Variable[a]
Cold crystallization		
T_{onset}		198–207 K
$\Delta_{cryst}H$		Variable[a]
Fusion of crystal **I**		
T_{onset}	264 ± 1.8 K	[b]
T_{peak}	270 ± 1.6 K	272.8 ± 0.10 K
$\Delta_{fus}H$	11.4 ± 0.80 kJ mol^{-1}	
Fusion of crystal **II**		
T_{onset}		260.4 ± 0.14 K
T_{peak}		268.5 ± 0.38 K
$\Delta_{fus}H$		8.4 ± 0.80 kJ mol^{-1}

[a] Measured values depend on the percentage of sample that vitrifies upon freezing. [b] Due to the overlapping between the onset side of the peak assigned to fusion of crystal **I** and the peak assigned to fusion of crystal **II** it was not possible to obtain a sufficiently accurate value for the onset temperature associated with fusion of crystal **I**.

indicate that these transitions are multi-step processes. Indeed, this is a common situation for organic molecules where hydrogen bonding interactions play important structural roles;[23] as it will be stressed later on, in the case of **MGly**, crystallization requires conformational reorganization and both intra- and intermolecular H-bond formation (or breaking), besides quenching of translational and rotational degrees of freedom.

The heating curve (b) shows several signals. A typical feature ascribable to a glass transition, with a negligible enthalpy change involved and an increase in the heat capacity, is observed at 174.6 ± 0.42 K. This means that upon rapid cooling a glassy state is formed in addition to crystalline phase **I**, the degree of crystallization depending on the sample history and, in particular, of the cooling rate. The small positive change of enthalpy, which appears superimposed with the change of heat capacity associated with this glass transition, reveals that some structural relaxation occurs during devitrification. This phenomenon has been previously observed for other systems.[23–25] The exothermic peak observed in curve (b) is characterized by an onset temperature in the range 198–207 K and corresponds to the formation of a new crystalline phase (crystal **II**), which is obtained from the glassy state in the presence of the crystalline phase **I**. The fusion peaks of the two crystalline varieties are observed at $T_{peak} = 272.8 \pm 0.10$ K (crystal **I**) and $T_{onset} = 260.4 \pm 0.14$ K, $T_{peak} = 268.5 \pm 0.38$ K (crystal **II**). Note that both the lower temperature of fusion of crystalline phase **II** and its slightly smaller enthalpy of fusion (8.4 ± 0.8 kJ mol^{-1}),† when compared with crystalline phase **I**, can be taken as indications that crystal **II** can be obtained at the expense of a small structural reorganization of the liquid (*i.e.*, it has a more relaxed structure with a slightly higher intrinsic energy than crystal **I**).

When fast cooling is used, successive cooling–warming cycles, carried out using the same conditions, lead to an increase in the amount of crystalline phase **I** formed during the cooling, relative to the glassy state. In particular, it is clear that the magnitudes of the observed changes in the heat capacities associated with the glass transition observed near 175 K correlate well with the absolute values of the enthalpy of crystallization on cooling the room temperature liquid to form crystal **I**, the smaller the heat capacity change, the larger the absolute value of the enthalpy of crystallization. Furthermore, as it could be expected, the absolute values of the enthalpy changes associated with the formation of crystal **II** from the glassy state (upon heating) also increase with the heat capacity changes associated with the glass transition.

In summary, DSC studies reveal that over the temperatures investigated **MGly** may exist in three solid phases. A stable crystalline phase (**I**) can be formed directly from the room temperature liquid upon slow cooling. Using faster cooling rates, a mixture of this crystalline phase and a glassy state is obtained, their relative amounts depending on the sample history. Under favorable conditions, a second crystalline variety (**II**) may also be formed by heating the low temperature glassy state. Such a crystalline state seems to have a more relaxed structure and a slightly higher energy than the crystalline phase **I**.

3.2 Vibrational spectroscopy (infrared and Raman) and molecular modeling studies

As mentioned in the Introduction, we have recently studied **MGly** by matrix isolation vibrational spectroscopy and *ab initio* quantum chemical calculations.[17] Our previous study provided a detailed understanding of the vibrational signature of the two conformers of this molecule that are experimentally observed both in the liquid phase and for the isolated molecule situation (conformers **Ss** and **Gsk**, see Fig. 1). In particular, some mark bands due to the individual conformers could be identified, which may be used as probes to identify the presence or measure the relative populations of these forms under different experimental conditions. The bands ascribed to the νC–C stretching mode are particularly suitable to this objective, since the two conformers give rise to relatively intense and well separated bands occurring in a clean spectral region (infrared: **Ss**, 892 cm^{-1}; **Gsk**, 846 cm^{-1}; Raman: **Ss**, 902 cm^{-1}; **Gsk**, 856 cm^{-1}).

The previous interpretation of the vibrational spectra of isolated **MGly** received a fundamental support from theoretical calculations (*ab initio* HF/6-31G* quantum chemical calculations[17]). However, the present study deals essentially with the solid state, where molecular aggregates and intermolecular interactions are expected to play important roles, and thus constitutes a considerably more complex system to be investigated. For this kind of system, the available quantum chemical methods that can provide *reliable* theoretical grounds for the interpretation of the observed spectroscopic data are still prohibitive in terms of computational needs. In these cases, classical molecular modeling methods (molecular mechanics) constitute a suitable alternative, which has been extensively tested in the past. Indeed, the most recent generation of force fields have been proved to be able to provide both structural and vibrational results whose agreement with experiment may be even better than currently practicable quantum chemical methods.[26,27]

In this study, the second generation CFF95 force field of Hagler and co-workers[21] was used. Table 2 compares the vibrational results obtained using this method for the conformational ground state of monomeric **MGly** (conformer **Ss**) with both experimental (matrix isolation; infrared) and *ab initio* HF/6-31G* (scaled values) data.[17] As can be noticed from Table 2, the CFF95 results show an excellent agreement with the experiment, in particular in what relates to frequencies (infrared intensities depend very much upon the

† To obtain the enthalpy of fusion of crystal **II**, the following procedure was used. Firstly, deconvolution of the two peaks appearing in DSC curves of type (b) in Fig. 2 was carried out and their corresponding areas were measured. Then, since the enthalpy of fusion of crystal **I** could be previously obtained from DSC curves of type (a) in Fig. 2 (11.4 ± 0.80 kJ mol^{-1}), the percentage of crystal **I** in each sample could be obtained. Assuming that only crystal **I** and crystal **II** co-exist before fusion, the amount of crystal **II** in each sample could be obtained and, then, the enthalpy of fusion of this crystalline phase determined.

Table 2 Experimental (Ar matrix) and calculated (*ab initio* HF/6-31G* and MM/CFF95) infrared vibrational spectra of methyl glycolate[a]

Approximate description	Conformer *syn-syn* s-*cis* (point group: C_S)						
	Experimental		Calculated				
	MI-IR		*Ab initio* HF/6-31G*		MM/CFF95		
	ν_{exp}/cm^{-1}	I_{exp}[b]	ν_{HF}/cm^{-1}	I_{HF}[c]	ν_{CFF95}/cm^{-1}	I_{CFF95}[d]	$\Delta\nu$[e]/cm^{-1}
νOH	3554	119	3633	98	3544	270	10
νCH_3 as′	3040	13	3004	24	2986	43	54
νCH_3 as″	3015	19	2986	28	2979	46	36
νCH_3 s	2967	43	2912	31	2896	12	71
νCH_2 as	2935	25	2911	34	2937	37	−2
νCH_2 s	2921	21	2881	30	2893	30	27
νC=O	1752	266	1793	318	1746	72	6
δCH_2	1463	31	1479	10	1473	52	−10
δCH_3 as′	1450[f]	28	1472	7	1467	6	−17
ωCH_2		37	1470	9	1413	29	37
δCH_3 as″	1445	18	1467	5	1446	26	−1
δCH_3 s	1440	18	1440	4	1428	103	12
νC–O	1277	269	1288	560	1281	201	−3
δCOH	1235	259	1256	75	1213	132	22
$twCH_2$	1219	3	1227	<1	1250	3	−31
$\rho CH_3'$	1191	6	1196	7	1145	12	46
$\rho CH_3''$	1159	3	1159	4	1123	6	36
νC–O(H)	1097	250	1097	194	1117	78	−20
ρCH_2	1018	4	1029	2	1006	29	12
$\nu O–C(H_3)$	991	48	997	33	985	55	6
νC–C	892	9	883	5	892	3	0
δO=C–O	691	20	681	26	682	34	9
ρC=O	576	32	571	42	590	34	−14
δCC=O	434	2	435	1	373	6	61
δCOC	343[g]	41	333	38	349	37	−6
τC–O(H)	303[g]	96	258	77	162	287	141
δOCC	225[h]		209	<1	213	6	12
$\tau O–C(H_3)$	120[h]		151	16	141	3	−21
τC–O	160[h]		131	7	196	3	−36
τC–C	85[h]		35	23	54	66	31

[a] ν, stretching; δ, bending; w, wagging; tw, twisting; ρ, rocking; τ, torsion; s, symmetric; as, asymmetric. [b] MI-IR intensities were normalized to the total calculated intensities of the bands which have an experimental counterpart by using the formula $I^{(i)}_{exp} = I^{(i)}_{obs} x \sum_{j=1,n} I^{(j)}_{HF} / \sum_{j-1,n} I^{(j)}_{obs}$, where the sums extend to all bands observed. [c] Calculated infrared intensities in km mol^{-1}. [d] MM/CFF95 intensities were normalized to the *ab initio* HF/6-31G*. [e] $\Delta\nu = \nu_{exp} - \nu_{CFF95}$. [f] Experimental intensities of the component bands were estimated by dividing the total observed intensity in consonance with their calculated intensity ratios. [g] From ref. 16. [h] Gas phase;[15] intensity not measured.

atomic charges and it is well known that these are extremely difficult to compute accurately by using molecular mechanics[28,29]). This result provides a very good test of the reliability of the CFF95 force field to calculate vibrational data for this kind of molecule, and justifies its use in the present study.

Fig. 3 and 4 show the experimental spectra obtained for both the stable crystalline phase **I** and the glassy state of **MGly**. These spectra are compared with the room temperature liquid phase spectra. The CFF95 predicted infrared spectrum for the crystalline phase is also shown in Fig. 3 (details of the calculation will be provided later on). Band assignments are shown in Tables 3 and 4.

The temperature variation Raman study was made by slowly cooling the sample initially at room temperature. By comparing the low temperature Raman spectra with that of the liquid, it is clear that those bands due to the higher energy form **Gsk**, which are easily observed in the liquid phase spectrum (*e.g.*, bands at 2862, 1016, 857, 670 and 503 cm^{-1}, assigned to δCH_3 s, $\nu O–C(H_3)$, νC–C, δO=C–O and δC–C=O, respectively; see Table 4), disappear in the solid state spectra. Spectroscopic results obtained after successive cooling–warming cycles did not lead to different conclusions.

Such results indicate that (i) the crystalline state attained corresponds to the stable crystalline phase **I**, (ii) under the experimental conditions used the whole sample crystallizes (so, the situation is similar to that corresponding to the DSC curve (a) in Fig. 2), and (iii) the crystalline phase formed exhibits conformational selectivity—in this phase, all individual molecules assume a conformation analogous to the most stable conformer found for the isolated molecule and in the liquid (the **Ss** form).

On the other hand, most of the bands in the Raman spectrum of the crystal appear as doublets. This indicates that the crystal shall exhibit two crystallographicaly non-equivalent types of molecules. We shall return to this point later on.

In the infrared experiments, the method used to prepare the sample was completely different, as described in the Experimental section: the KBr substrate was first cooled down to 13 K and then **MGly** vapour was sprayed onto the cold window. As could be expected, the infrared spectrum of the thin film formed in this way (see Fig. 3) clearly shows that a glassy state was produced. In the glassy state spectra, mark bands of both **Ss** and **Gsk** conformers are easily observable, showing that in this phase **MGly** individual molecules may assume the two conformational states previously observed for this compound isolated in an argon matrix and in the room temperature liquid phase.[17] Increasing the temperature does not produce any significant changes in the infrared spectrum until the temperature reaches a value close to the temperature of the cold crystallization detected by DSC. Then, (i) all mark bands of conformer **Gsk** disappear, (ii) most of the bands split into doublets, and (iii) there is an extensive reorganization of the profile of the bands in the νOH region (see Fig. 3). All these

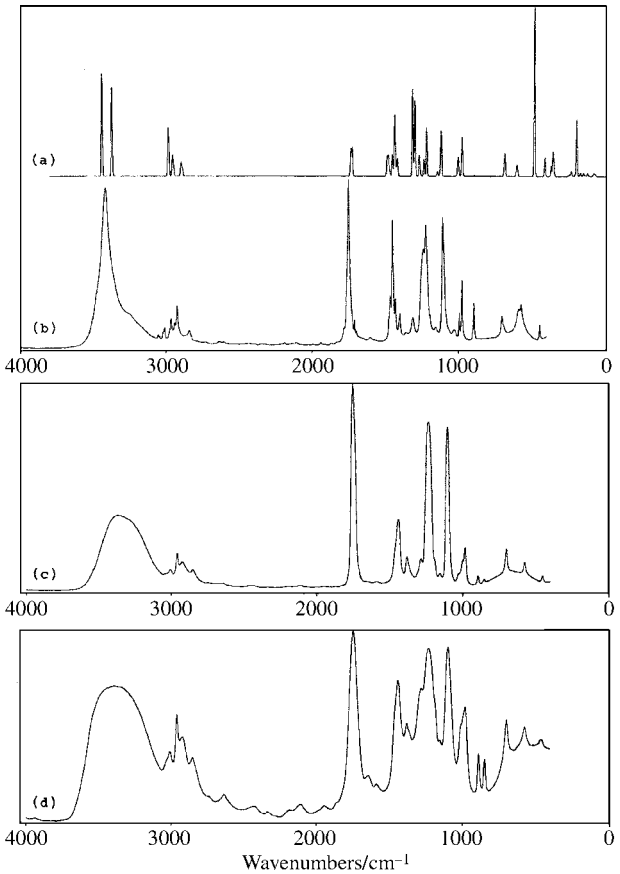

Fig. 3 Infrared spectra of methyl glycolate. (a) CFF95 calculated spectrum, (b) crystalline phase **I** ($T = 200$ K), (c) glassy state ($T = 65$ K) and (d) liquid ($T = 298$ K).

changes indicate that the glassy state initially formed was converted to crystalline phase **I**.

It is particularly interesting that under these experimental conditions, where only the glassy state is initially present in the sample, crystal **I** is formed upon warming instead of crystal **II**, which is the product observed when the glassy state initially coexists with crystalline phase **I**. Hence, it may be concluded that heteronucleation is a relevant factor to induce formation of the metastable crystalline phase **II** from the glassy state and that crystal **I**, in particular, may efficiently act as a nucleation agent for this process.

In order to identify the most important intermolecular interactions between **MGly** molecules, which are essential to determine the structures of the crystalline phases, a systematic search on the CFF95 potential energy surface of the dimer was undertaken (monomeric units were considered to assume a nearly **Ss** conformation, in consonance with the experimental data). It is assumed here that the dimer should constitute the basic structural associate within the crystalline unit cells. The most stable dimeric structures found are shown in Fig. 5. The lowest energy associate ($\mathbf{D^I}$) belongs to the symmetry point group C_i and has an inversion centre in the midle of the ten atom ring resulting from the establishment of two equivalent OH···O′= intermolecular hydrogen bonds made between the hydroxy group of one molecule and the carbonyl oxygen atom of the second molecule. The second more stable dimeric structure ($\mathbf{D^{II}}$; C_1 point group) is an open chain dimer, with a single intermolecular hydrogen bond ($\Delta E_{\mathbf{D^{II}D^I}} = 3.45$ kJ mol^{-1}). Finally, the highest energy form ($\mathbf{D^{III}}$; $\Delta E_{\mathbf{D^{III}\_D^I}} = 7.70$ kJ mol^{-1}) exhibits an eight atoms ring and, as $\mathbf{D^{II}}$, belongs to the C_1 point group, showing non-equivalent OH and C=O groups.

Once the structures of the most stable dimers were obtained, simulation of crystalline phases based on these dimers was undertaken. Full optimization of periodic structures containing the smaller number of molecules which can give rise to the observed vibrational spectra was systematically done and the calculated spectra compared with the observed data obtained for crystal **I**. All fundamental lattice parameters (axes and angles) were let free to vary independently during the optimization process, the most stable structures found belonging to the space group P_1. Since in the experimental vibrational spectra most of the bands appear as doublets, two dimeric units were used in setting up the periodic structures used to simulate the crystal, when $\mathbf{D^I}$ was used, while in the case of the periodic structures based on $\mathbf{D^{II}}$ and $\mathbf{D^{III}}$ a single dimeric unit was considered. Amongst all the periodic structures studied, the most stable one was found to be based on $\mathbf{D^{II}}$, being more stable than the most stable periodic structures based on $\mathbf{D^I}$ or $\mathbf{D^{III}}$ by more than 50 kJ mol^{-1}. In this structure, the two non-equivalent molecules of **MGly** that form the basic dimeric unit assume nearly **Ss** conformations with an *intra*molecular OH···O= hydrogen bond, and are connected by a relatively strong *inter*molecular OH···O′= hydrogen bond [d(OH···O′=) = 200.9 pm]. The

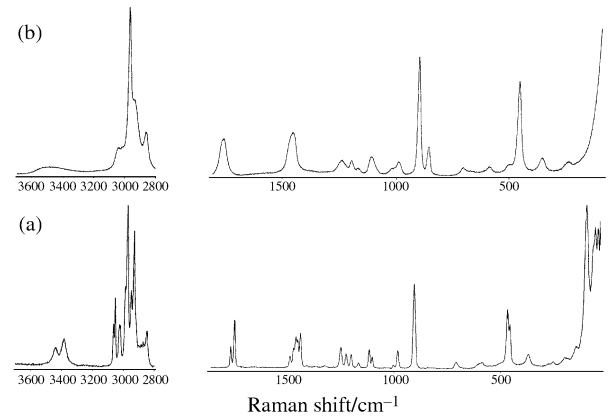

Fig. 4 Raman spectra of methyl glycolate. (a) Crystalline phase **I** ($T = 200$ K) and (b) liquid ($T = 298$ K).

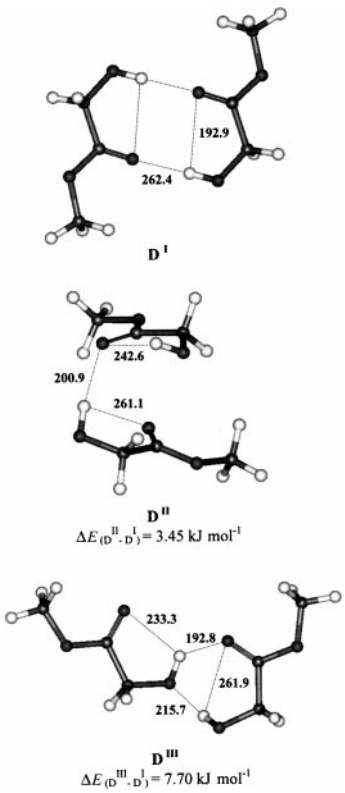

Fig. 5 Most stable dimers of methyl glycolate. Calculated hydrogen bond distances in pm.

Table 3 Experimental and calculated frequencies and intensities for methyl glycolate crystalline phase **I**[a]

Approximate description	Calculated (MM/CFF95)						Experimental							
							Infrared				Raman			
	ν_{CFF95}[b]/cm^{-1}		ν_{corr}[c]/cm^{-1}		I_{CFF95}[d]		ν_{exp}/cm^{-1}		I_{exp}[e]		ν_{exp}/cm^{-1}		I_{exp}[f]	
νOH	3436	*3368*	3446	*3378*	175	152	3416	*3366*			3444	*3387*	50	47
νCH_3 as′	2984	*2977*	3038	*3031*	29	29	3055	*3045*	3	1	3066	*3055*	21	21
νCH_3 as″	2983	*2980*	3019	*3016*	32	23	3019	*3010*	4	9	3029	*3021*	19	11
νCH_3 s	2898	*2892*	2969	*2963*	9	6	2980	*2966*	1	26	2991	*2977*	39	87
νCH_2 as	*2953*	2945	*2951*	2943	34	17	2941		24		2952		67	
νCH_2 s	*2893*	2885	*2920*	2912	14	11	*2923*	2909	42	7	*2934*	2920	63	8
νC=O	*1733*	1724	*1739*	1730	46	49	*1750*	1741	172	125	*1760*	1744	16	36
δCH_2	*1485*	1477	*1475*	1467	32	32	*1475*	1466	9	39	*1487*	1471	9	15
δCH_3 as′	1471	*1468*	1454	*1451*	6	9	1461		2		1461		27	
ωCH_2	1419	*1415*	1456	*1452*	14	23	1449	*1441*	129	19	1452		19	
δCH_3 as″	1449	*1448*	1448	*1447*	26	11	1430	1426	13	26	1438		31	
δCH_3 s	1434	*1430*	1446	*1442*	77	49	1399		30		1409		2	
νC–O	*1311*	1296	*1308*	1293	149	129	*1356*	1309	12	33	*1368*	1323	1	2
δCOH	*1234*	1216	*1256*	1238	29	83	*1254*	1240	49	118	*1253*	1249	10	12
$twCH_2$	*1265*	1260	*1234*	1229	34	6	*1122*	1213	118	97	1225		14	
$\rho CH_3'$	*1144*	1141	*1190*	1187	3	6	*1192*	1185	6	1	1202		10	
$\rho CH_3''$	1124	*1123*	1160	*1159*	6	2	1157	*1150*	3	3	1169	*1163*	4	1
νC–O(H)	*1117*	1116	*1097*	1096	46	32	*1107*	1097	102	68	*1118*	1104	17	9
ρCH_2	1005	*1011*	1017	*1013*	11	26	1029	*1018*	10	1	1005		1	
$\nu O–C(H_3)$	978	*973*	984	*979*	20	57	993	*974*	13	42	986		15	
νC–C	*893*	892	*893*	892	<1	1	*900*	892	3	19	*911*	903	59	41
δO=C–O	688[i]	683[o]	697[i]	691[o]	14	32	703[i]	697[o]	7	22	711	700	6	1
ρC=O	606	*600*	592	*586*	9	17	589	*571*	28	7	585	*564*	4	3
τC–O(H)	484[i]	413[o]	625[i]	554[o]	287	32	652[i]	570[o]	67	106	600[i]	552[o]	55	26
δCC=O	*380*	370	*441*	431	<1	17	447		8		*470*	457	23	7
δCOC	357	*352*	351	*346*	34	17	n.i.	n.i.	n.i.	n.i.	373	*369*	11	1
δOCC	*246*	234	*258*	246	3	9	n.i.	n.i.	n.i.	n.i.	*276*	254	5	9
τC–O	209[o]	198[i]	173[o]	162[i]	3	98	n.i.	n.i.	n.i.	n.i.	199	179	32	
$\tau O–C(H_3)$	181	*152*	160	*131*	<1	6	n.i.	n.i.	n.i.	n.i.	142		27	7
τC–C	111[o]	90[i]	142[o]	121[i]	<1	1	n.i.	n.i.	n.i.	n.i.	n.o.		n.o.	n.o.

[a] ν, stretching; δ, bending; ω, wagging; tw, twisting; ρ, rocking; τ, torsion, s, symmetric; as, asymmetric; n.o., not observed; n.i., non-investigated. Wavenumber values shown in *italic* refer to bands due to the molecule within the dimeric unit which acts as hydrogen bond acceptor, when both molecules within the dimer contribute significantly to the vibration, this is notated as in-phase (superscript i) or out-of-phase (superscript o). [b] Calculated frequencies for intermolecular H-bonding and lattice vibrations (not experimentally investigated) are 140, 127, 124, 90, 82, 72, 50, 44 and 39 cm^{-1}. [c] $\nu_{corr} = \nu_{CFF95} + \Delta\nu$, where $\Delta\nu$ is the difference between the experimental and MM/CFF95 calculated frequencies found for the monomers (see Table 2). [d] Calculated intensities were scaled using the factor determined for the monomer: 2.87. [e] Infrared experimental intensities were normalized to the total calculated intensities (I_{CFF95}) of the bands which have an experimental counterpart by using the formula $I^{(i)}_{exp} = I^{(i)}_{obs} \times \sum_{j=1,n} I^{(j)}_{CFF95} / \sum_{i=1,n} I^{(j)}_{obs}$, where the sums extend to all bands observed; νOH bands were excluded, since it is clear that calculations strongly underestimate intensities (using the same factor, the experimental intensities for the νOH bands would be 822 and 399, respectively, for the high and low frequency band). [f] Raman intensities are normalized intensities (to 1000).

calculated vibrational data for this periodic structure is shown in Table 3 and Fig. 3 and, as it can be noticed, agree very well with the experimental results. It is worth noting that the calculated vibrational spectra obtained for other periodic structures of relatively low energy, in particular the most stable structures based on $\mathbf{D^I}$ and $\mathbf{D^{III}}$, do not fit well to the experimental data. For instance, for the most stable periodic structure, the absolute error between the calculated and experimental vibrational frequencies for those modes associated with the groups which are directly involved in hydrogen bonding is 96 cm^{-1}, whereas the minimum error for a $\mathbf{D^I}$ or $\mathbf{D^{III}}$ based periodic structure was found to be 244 cm^{-1} (calculated OH bending frequencies show particularly large deviations from the observed values, indicating that the hydrogen bonding network of the crystal is not properly described by such structures). Hence, despite the simplicity of the model used here to simulate the observed crystalline phase of **MGly**, it can be concluded that with all probability crystalline phase **I** is based on $\mathbf{D^{II}}$.

Considering the good general agreement between the calculated and experimental vibrational frequencies‡ now obtained and the general discussion of the liquid phase and matrix isolation spectra of **MGly** we presented elsewhere,[17] a detailed analysis of the assignments made here does not seem necessary. However, some specific spectral regions deserve further comment.

OH stretching (*ν*OH) region. As is usual for hydroxy containing molecules participating in H-bonding, in the liquid phase spectra of **MGly** νOH appears as a very broad band, which is very intense in the infrared spectrum and much weaker in the Raman spectrum. Increasing the temperature leads to an increase of the high frequency side of the νOH infrared band, in agreement with an increase of the population of conformer **Gsk**, where this vibration has been shown to occur at a higher frequency than in the most stable form.[17] In the glassy state, the spectral profile in this region is similar to that observed in the liquid state. On the other hand, in the Raman spectrum of the crystalline phase **I**, a doublet of bands is clearly observed at 3444 and 3387 cm^{-1}. These bands, that are predicted by the calculations to appear at 3446 and 3378 cm^{-1}, have infrared counterparts at 3416 and 3366 cm^{-1}. Deconvolution of the infrared spectrum of the crystal shows that, besides the two main bands ascribed to the νOH fundamentals, additional bands of lower intensity are presented in this spectral region. These bands are tentatively assigned to the first overtones of the carbonyl stretching modes, which are

‡ As mentioned before, intensities are usually not very well predicted by molecular mechanics,[28,29] and the calculated data just exhibit a rough agreement with experiment.

Table 4 Experimental frequencies and intensities for methyl glycolate liquid and glassy states[a]

Approximate description	Liquid phase				Glassy state	
	ν_{ir}/cm^{-1}	I_{ir}	ν_{Raman}/cm^{-1}	I_{Raman}	ν_{ir}/cm^{-1}	I_{ir}
νOH	3393	s, b	3350–3350	w, b	3368	s, b
νCH_3 as′	3041	vw, sh	3042	m	3036	w
νCH_3 as″	3013	w	3021	m	3006	w
νCH_3 s	2959	m	2968	s	2958	m
νCH_2 as	2919	m	2938	m	2925	m
νCH_2 s	2919	m	2938	m	2925	m
	2852[b]	w	*2861*[b]	m	*2850*[b]	w
νC=O	1750	s	1751	m	1755	vs
δCH_2 / δCH_3 as′ / ωCH_2	1460	m, sh	1454	m	1460	m, sh
δCH_3 as″	1441	m	1454	m	1438	m
δCH_3 s	1383	w	1382	vw	1379	m
	1364	w, sh	n.o.		*1368*	w, sh
νC–O	*1298*	w, sh	n.o.		*1293*	w, sh
	1280	m	1301	vw	1283	m
δCOH	1241	s	1241	w	1242	s
$twCH_2$	1215	s	1232	w	1220	s
$\rho CH_3'$	1194	m, sh	1196	w	1190	w, sh
$\rho CH_3''$	1148	vw	1165	vw	1154	vw
νC–O(H)	1099	s	1109	w	1102	s
ρCH_2	1009	w, sh	1020	vw	1024	w
$\nu O–C(H_3)$	*1009*	w, sh	*1016*	vw, sh	*998*	m
	981	m	990	w	980	m
νC–C	892	w	900	s	892	w
	846	w	*856*	m	*849*	w
τC–O(H)	*772*	vw, sh	n.o.		*772*	w, b
	618	w	618	vw, sh	640	w, b
δO=C–O	699	w	706	w	699	m
	663	vw	*680*	vw	*688*	vw
ρC=O	579	w	591	w	575	m
δCC=O	*510*	w	*508*	w	*501*	vw, sh
	450	vw	458	s	453	w
δCOC	350	s	357	w	n.i.	
δOCC	n.i.		294	w	n.i.	
$\tau O–C(H_3)$	n.i.		n.o.[d]		n.i.	
τC–O	n.i.		n.o.[d]		n.i.	
τC–C	n.i.		n.o.[d]		n.i.	

[a] ν, stretching; δ, bending; ω, wagging; tw, twisting; ρ, rocking; τ, torsion; s, symmetric; as, asymmetric; n.o., not observed; n.i., not investigated. Intensities are presented in a qualitative way: vs, very strong; s, strong; m, medium; w, weak; vw, very weak; sh, shoulder; b, broad. Data shown in *italic* correspond to bands assigned to conformer **Gsk**. [b] This band also contains a significant contribution due to the first overtone of the δCH_3 as; bending vibration in Fermi resonance with νCH_3 s. [c] From ref. 13. [d] Overlapped by the Rayleigh line.

with all probability in Fermi resonance with the νOH fundamentals.

CO stretching modes (*ν*C=O, *ν*C–O, *ν*C–O(H) and *ν*O–C(H_3)). The carbonyl stretching vibration could be assigned easily in all spectra. In both the liquid and glassy state, a single unresolved band resulting from the νC=O vibrations of the two conformers was observed (liquid: 1750 cm^{-1}; glassy state: 1755 cm^{-1}). In the spectra of crystalline phase **I** this mode is assigned to the doublets appearing at 1750 and 1741 cm^{-1}, in the infrared, and at 1760 and 1744 cm^{-1}, in the Raman. The remaining three CO stretching vibrations, νC–O, νC–O(H) and νO–C(H_3), are predicted to occur in the crystalline phase **I** as doublets near 1300, 1100 and 980 cm^{-1}, respectively. In the infrared spectrum, where they are predicted to give rise to intense features, all expected bands could be easily observed (νC–O: 1356, 1309 cm^{-1}; νC–O(H): 1107, 1097 cm^{-1}; νO–C(H_3): 993, 974 cm^{-1}]. As shown in Table 3, the experimental and calculated data for these modes agree very well. It is also worth mentioning that no sigificant frequency shifts are observed for either νC–O(H) or νO–C(H_3) when compared with the isolated molecule situation—where these vibrations were found to give rise to bands at 1097 and 991 cm^{-1}, respectively,[17]—while νC–O is appreciably blue shifted in the crystalline state, as could be expected taking into consideration the increase in the double bond character of the C–O bond associated with the increased importance of canonical form **II**, shown in Fig. 6, in this phase, due to the involvement of the carbonyl group in intermolecular hydrogen bonding and the higher polarity of the media[30] (νC–O in the isolated molecule situation occurs at 1277 cm^{-1} [17]).

In the liquid phase as well as in the glassy state, νC–O(H) and νO–C(H_3) appear at frequencies that are also similar to those observed for the isolated molecule situation, but in the case of νO–C(H_3), the band originated in conformer **Gsk** could also be observed experimentally (liquid phase: 1009 cm^{-1}; glassy state: 998 cm^{-1}; see Table 4). In these phases, νC–O due to form **Ss** gives rise to a band at 1280 cm^{-1} (liquid phase) or 1283 cm^{-1} (glassy state), thus appearing at a frequency in between those observed for the isolated molecule and in crystalline phase **I**. These results indicate that the rela-

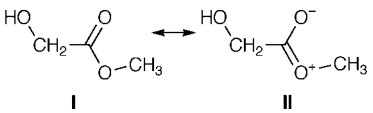

I II

Fig. 6 Canonical forms of methyl glycolate showing the mesomerism within the carboxylic ester group.

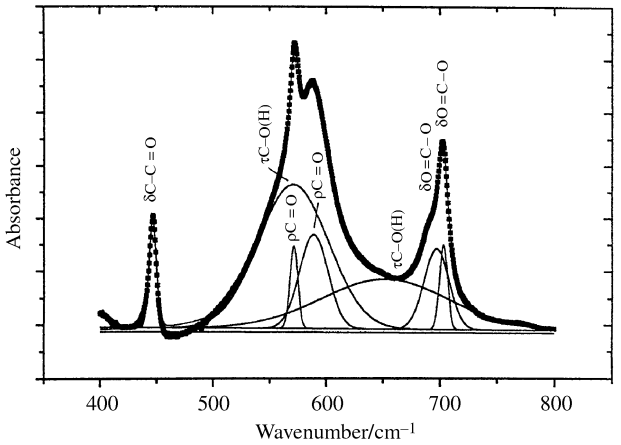

Fig. 7 400–800 cm^{-1} spectral region (deconvoluted using gaussian functions) of the infrared spectrum of methyl glycolate in the crystalline phase **I** ($T = 200$ K).

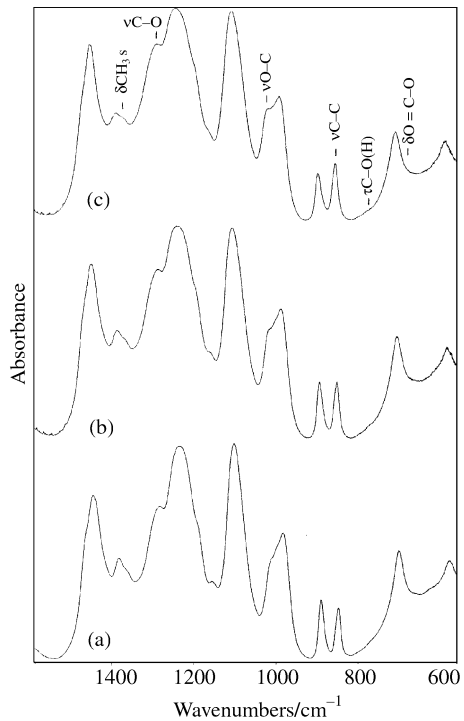

Fig. 8 1550–550 cm^{-1} spectral region of the infrared spectrum of liquid methyl glycolate as a function of temperature. (a) $T = 298$ K, (b) $T = 318$ K and (c) $T = 398$ K. Those bands due to the less stable conformer (Gsk) or having a predominant contribution from this form are marked.

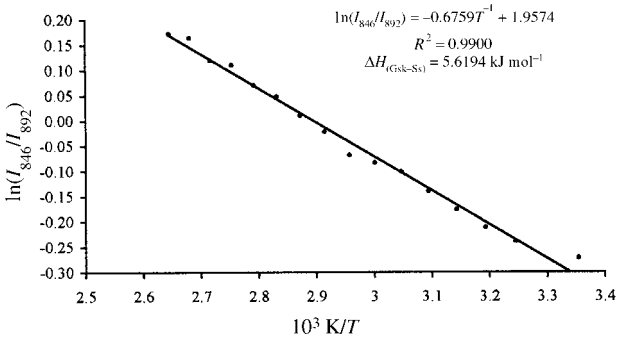

Fig. 9 Van't Hoff plot [$\log(I_{846}/I_{892})$ *vs.* T^{-1}], showing the temperature dependance of the relative intensities of the infrared *ν*C–C stretching bands assigned to conformers Ss (892 cm^{-1}) and Gsk (846 cm^{-1}).

tive importance of canonical form **II** of Fig. 6, which, as mentioned before, provides a good indication of the local polarity arround the carboxylic ester group and may also be used to estimate the relative strength of hydrogen bonding, increases in the order: isolated molecule < liquid < glassy state- < crystal **I**. In the infrared spectra of the liquid and of the glassy state, it is also possible to observe the band due to the νC–O vibration of the **Gsk** conformer, which in both cases appears as a shoulder near 1295 cm^{-1}.

COH in-plane (*δ*COH) and out-of-plane (*τ*C–O(H)) bending vibrations. Conformer **Ss** of **MGly** isolated in an argon matrix gives rise to a very intense δCOH infrared band at 1235 cm^{-1}.[17] Following the trend previously observed for other hydroxylic molecules,[30] this vibration appears at a higher frequency in the crystalline state (infrared: 1254, 1240 cm^{-1}; Raman: 1253, 1249 cm^{-1}) as well as in the liquid and glassy states (1241 and 1242 cm^{-1}, respectively). Note that, as expected, the extension of the blue shifts observed for this vibration in the various phases studied relative to the isolated molecule situation, follows the same order of the above discussed relative increase in frequency of the νC–O mode.

A more pronounced blue shift upon going from the isolated molecule situation towards the condensed phases could be expected to occur for the τC–O(H) mode.[30] In the matrix isolated **Ss** conformer of **MGly**, this mode gives rise to an intense infrared band at 303 cm^{-1}.[17] Not very surprisingly, in the condensed phases, τC–O(H) was found to give rise to very broad bands appearing at frequencies above 550 cm^{-1} (see Tables 3 and 4). Fig. 7 shows the deconvoluted infrared spectrum of crystalline phase **I** in the region where the τC–O(H) bands appear.

Temperature studies in the liquid phase. As mentioned before, in our previous study on liquid **MGly** no temperature variation studies were undertaken, and the conformational population ratio then estimated was obtained taking only into consideration the comparison between the calculated and observed relative intensities of the νC–C stretching Raman bands originated in each conformer.[17] To improve the available description of the conformational equilibrium in this phase, a temperature variation study of the liquid phase infrared spectrum of **MGly**, within the temperature range 273–373 K, was undertaken in the present study. The results obtained are shown in Fig. 8 and 9. Besides confirming the previous assignment of the bands appearing at 2852, 1364, 1298, 1009, 846, 772, 663 and 510 cm^{-1} to conformer **Gsk** (see Fig. 8), an experimental value for the **Gsk**/**Ss** population ratio in the pure liquid, at 298 K, could be obtained from the Van't Hoff plot shown in Fig. 9. The value now obtained (0.207, which corresponds to $\Delta H_{(\mathbf{Gsk\text{-}Ss})} = 5.62 \pm 0.02$ kJ mol^{-1}), is somewhat lower than our previous estimation (0.457[17]). However, this value is still in consonance (and reinforces) the interpretation previously made to explain the observed increase in the population of the **Gsk** form in the liquid when compared with the gas phase at the same temperature (**Gsk**/**Ss** = 0.043[17]): conformer **Gsk** is stabilized in the liquid relative to conformer **Ss** because it is able to participate in stronger *inter*molecular hydrogen bonds than this latter form, where *inter*molecular H-bonding must compete with a considerably stronger *intra*-molecular OH···O= hydrogen bond.

Acknowledgements

The authors acknowledge Dr João Cecílio for his technical help. This work has been carried out within the PRAXIS XXI (QUI/2/2.1/412/94) research programme that is also partially funded by FEDER.

References

1 E. V. Scott, *J. Am. Acad. Derm.*, 1984, **11**, 867.
2 Y. Guzel, *THEOCHEM*, 1996, **366**, 131.
3 L. Moy, H. Murad and R. L. Moy, *J. Derm. Surg. Oncol.*, 1993, **19**, 243.
4 E. V. Scott, *Can. J. Derm.*, 1989, **43**, 222.
5 D. J. Mooney, *Proceedings of the 1996 fifteenth southern biomedical engineering conference*, New York, 1996.
6 N. L. Allinger, M. P. Cava, D. C. de Jongh, C. R. Johnson, N. A. Lebel and C. L. Stevens, *Química Orgânica*, Guanabara, Rio de Janeiro, 1978, and references therein.
7 C. E. Blom and A. Bauder, *J. Am. Chem. Soc.*, 1982, **104**, 2993.
8 H. Hasegawa, O. Ohashi and I. Yamaguchi, *J. Mol. Struct.*, 1982, **82**, 205.
9 H. Hollenstein, T. K. Ha and Hs. H. Günther, *J. Mol. Struct.*, 1986, **146**, 289.
10 K. Iijima, M. Kato and B. Beagley, *J. Mol. Struct.*, 1993, **295**, 289.
11 H. Hollenstein, *J. Mol. Struct.*, 1982, **79**, 447.
12 Z. Smedarchine and F. Zerbetto, *Chem. Phys. Lett.*, 1997, **271**, 189.
13 G. Cassanas, M. Morssli, E. Fabrégue and L. Bardet, *J. Raman Spectrosc.*, 1991, **22**, 11.
14 W. Caminati, R. Cervellati and Z. Smith, *J. Mol. Struct.*, 1983, **97**, 87.
15 R. Mayer, W. Caminati and H. Hollenstein, *J. Mol. Spectrosc.*, 1989, **137**, 87.
16 H. Hollenstein, R. W. Schar, N. Schwizgebel, G. Grassi and Hs. H. Günthard, *Spectrochim. Acta, Part A*, 1983, **39**, 193.
17 S. Jarmelo and R. Fausto, *J. Mol. Struct.*, 1999, **509**, 183.
18 Microcal origin (version 4.0), © copyright 1991–1995, Microcal software, Inc.
19 F. A. Miller and B. M. Harney, *Appl. Spectrosc.*, 1970, **2**, 291.
20 R. Sabbah, A. Xu-Wu, J. S. Chickos, M. L. P. Leitão, M. V. Roux and L. A. Torres, *Thermochim. Acta*, 1999, **331**, 93.
21 (*a*) A. T. Hagler and C. S. Ewig, *Comput. Phys. Commun.*, 1994, **84**, 131; (*b*) M. J. Hwang, T. P. Stockfish and A. T. Hagler, *J. Am. Chem. Soc.*, 1994, **116**, 2515.
22 Cerius2 (version 3.5), Molecular Simulations Inc., San Diego, CA, 1997.
23 J. C. C. Lage, PhD Thesis, University of Coimbra, Portugal, 1999, and references therein.
24 M. R. Richardson and N. G. Savill, *Polymer*, 1975, **16**, 753.
25 M. J. Richardson, *Plast. Rubber: Mater. Appl.*, 1976, **1**, 162.
26 U. Burket and N. L. Allinger, *Molecular Mechanics*, ACS Monograph 177, American Chemical Society, Washington, USA, 1982.
27 A. Soldera and J. P. Dognon, *Macromol. Symp.*, 1997, **119**, 157.
28 R. Fausto, *Rev. Port. Quím.*, 1996, **3**, 59.
29 K. Rasmussen, *Potential Energy Functions in Conformational Analysis*, *Lecture Notes in Chemistry*, Springer-Verlag, Heidelberg, 1985, vol. 37.
30 R. Fausto, *J. Mol. Struct.*, 1996, **377**, 181.

Paper a909291i